A Computational Study of Combustor Dilution Flow Interaction with Turbine Vanes

Kirsten Muirhead*
Stephen Lynch†
The Pennsylvania State University
University Park, PA 16802

Higher efficiency and greater performance in gas turbine engines can be achieved by increasing the combustion temperature to increase power output, but is limited by durability concerns for downstream hardware. In many aircraft combustors, large-scale dilution cooling flows are injected to complete combustion and mix out hot spots. However, if not properly designed, spatial and temporal non-uniformities in flow and temperature caused by the jets can propagate downstream to the first row of turbine vanes. The non-uniform thermal loading can cause damage to vanes and increase maintenance costs. Several previous studies have examined the mean and turbulent velocity and temperature profiles at the exit of a combustor, but the temporally and spatially resolved effect of dilution jets on the turbine vane surface heat transfer has not been widely studied. This work computationally modeled the flow in a non-reacting combustor simulator, in both time-average (steady Reynolds Averaged Navier Stokes, RANS) and time-dependent (Delayed Detached Eddy Simulation, DDES) analyses. The effects of various dilution hole configurations on the temperature of downstream components was studied in the time-average approach. Configurations where the dilution jets were closer to the vane resulted in significant flow non-uniformity at the turbine inlet, and large gradients in adiabatic wall temperature of the vane. Neither the steady or unsteady computational methods captured the observed behavior of the turbulent dilution jets; however, there was a significant difference between the predicted vane temperature. Refinement of the time-dependent analysis in a region around the dilution jets did not significantly change the predicted turbine inlet flowfield.

Nomenclature

$k = turbulent\ kinetic\ energy;\ \ k = \frac{1}{2}\left(\overline{u'^2} + \overline{v'^2} + \overline{w'^2}\right)$

$I =\ momentum\ flux\ ratio\ between\ jet\ and\ freestream;\ I = \frac{\rho_c V_c^2}{\rho_\infty V_\infty^2}$

$t = time$

$T_c = coolant\ temperature$

$T_\infty\ = freestream\ temperature$

$u = axial\ velocity\ (x - direction)$

$v = pitchwise\ velocity\ (y - direction)$

$w = spanwise\ velocity\ (z - direction)$

$U = time - average\ axial\ velocity$

$U_{in} = domain\ inlet\ velocity$

$\bar{U} = mass - average\ turbine\ inlet\ axial\ velocity\ (space\ and\ time - average)$

$V_c = coolant\ velocity$

$VR = velocity\ ratio\ between\ jet\ and\ freestream; VR = \frac{V_c}{V_\infty}$

$X, Y, Z = global\ coordinates\ (axial, pitchwise, spanwise)$

Greek

$\theta = nondimensional\ temperature;\ \theta = \frac{T_\infty - T}{T_\infty - T_c}$

$\varepsilon = dissipation\ rate\ per\ unit\ mass$

$\eta = Kolmogorov\ length\ scale\ (Eq. 1)$

---

* Undergraduate Student, Aerospace Engineering, AIAA Student Member
† Assistant professor, Mechanical Engineering, AIAA Senior Member

$\nu = viscosity$
$\rho_c = coolant\ density$
$\rho_\infty = freestream\ density$

Superscript/Subscript
$\overline{()'} = RMS\ of\ quantity$

I. Introduction

Gas turbine engine efficiency can be improved by increasing the combustion temperature, and by decreasing the amount of uncombusted cooling air required to prevent component overheating. More effective component cooling with less coolant requires a more precise understanding of thermal loads on hot-section components. The first row of nozzle guide vanes downstream of the combustor are subjected to some of the highest heat loads in the engine. They are cooled with film cooling on the vane outer surfaces (small-scale coolant flows) as well as internal cooling through interior channels. However, the amount of vane cooling required is highly dependent on the incoming conditions, including both the distribution of the temperature field as well as the turbulence of the flow.

In a typical aeroengine Rich-Quench-Lean (RQL) style combustor, turbulent flow is desirable to provide adequate mixing for completion of combustion as well as for dilution of hot products. Dilution cooling is accomplished by injecting uncombusted air into the combustor through large holes in the casing. These jets-in-crossflow produce turbulent vortical structures in their wakes and within the jet itself (Fric and Roshko [1]). The turbulence mixes and homogenizes the combusted flow, but some turbulent structures propagate downstream.

In industry, combustor modeling has evolved to capture the important dynamical motions of the flow via turbulent scale-resolving methods. However, in the turbine design, the spatial and temporal variation of these structures are often neglected and the turbine inlet condition is reduced to an area-average value, or possibly a circumferentially-averaged profile (Barringer et al. [2]). Flow through the turbine inlet plane is not only non-uniform in space, but also in time, resulting in non-uniform, time-variant thermal loading on the vanes. These non-uniformities may be further exacerbated by the reduction of gas turbine core size for next-generation ultra high bypass ratio engines (Epstein [3]), where the combustor may need to be even more compact. Understanding these effects is important to optimize cooling, so that gains in propulsive efficiency from high bypass ratios are not offset by losses in engine thermodynamic efficiency due to increased cooling requirements.

This computational study examines the effect of dilution flow interaction with a downstream turbine vane, based on a simplified geometry studied experimentally by Vakil and Thole [4]. The effect of dilution hole location is investigated using a steady Reynolds-Averaged Navier-Stokes (RANS) approach. The importance of a turbulent scale-resolving (Delayed Detached Eddy Simulation, DDES) approach is investigated for the baseline experimental dilution configuration, and the impact of refining the DDES model is tested.

II. Previous Studies

Several studies have compared the effects of dilution hole parameters on time-average combustor exit flowfields. Holdeman and Walker [5] studied the effects of momentum flux ratios, diameter ratios, density ratios, and downstream distance of injection on jet penetration and temperature profiles of a single row of jets. Momentum flux ratio and diameter ratio proved to be the dominant variables, with penetration and mixing increasing with increasing momentum ratio and increasing jet diameter. Holdeman et al. [6] studied the mixing length of opposed and offset rows of jets more representative of a gas turbine combustor and found that opposed configurations were most effective in homogenizing the temperature field downstream. Stevens and Carrotte [7] studied the effects of equally-spaced jets in an annulus and discovered that the counter-rotating vortex pair is randomly asymmetrical. The twisting temperature contours that result are responsible for pitchwise asymmetry of the temperature distribution. The counter-rotating vortex pair dominates the flowfield downstream of the dilution jets. Stevens and Carrotte [8] further investigated the effects of jets in crossflow and concluded that the flowfield varies randomly from one jet to another and causes each jet to have its own mixing characteristics. This is responsible for the irregularity of the temperature within the annulus.

Dai et al. [9] studied multiple jets in confined crossflow and compared the effectiveness of directly opposed and staggered configurations. In the near field, directly opposed jets have better initial mixing than staggered jets at their respective optimum conditions. However, properly spaced staggered jets form a different vortex pattern, and the temperature and velocity contours at the combustor exit are more uniform relative to opposed jets. The staggered jets produce a larger length scale counter-rotating vortex pair that increases mixing. Barringer et al. [2] measured exit profile conditions with and without dilution flow in the low-speed recirculating wind tunnel combustor simulator modeled in this study. The results of the study invalidated the common assumptions of either a constant total pressure

field or a turbulent boundary layer for vane inlet conditions, and found that turbulent length scales exiting the combustor were on the order of the dilution jet diameter.

Some studies have investigated combustor flowfields in more detail. Vakil and Thole [4] measured thermal fields and mean and fluctuating velocities generated by the dilution jets in the same combustor simulator of Barringer et al. [2]. Kidney-shaped thermal fields were present, indicating the presence of counter-rotating vortex pairs. The directly-opposed dilution jets in that study impacted one another, evidenced by the spreading of the kidney-shaped contours in the mainstream. A recent study by Cha et al. [10] examined the nozzle guide vane inlet plane using an annular combustor simulator. The study concluded that the turbine inlet is dominated by the upstream dilution jet dynamics, is highly turbulent, and highly nonuniform in regards to temperature distribution. However, there were no measurements shown for the vane.

Computational modeling of combustor flowfields is now commonly done using high-fidelity methods such as Large Eddy Simulation (LES) or related variants (Di mare et al. [11], Moin and Apte [12], Patil and Tafti [13], Boudier et al. [14]), to capture the complex fluid dynamics and chemistry that occurs. Cha et al. [15] reported that time-averaged LES and RANS calculations of velocity and turbulence intensity at the turbine inlet agree with experimental trends, with LES producing more accurate data than RANS. Peak turbulence intensities at the turbine inlet plane are approximately 35%, with turbulence generated mainly by dilution jets. However, high-fidelity CFD has not yet become as common for the turbine, due to the much higher Reynolds numbers that are computationally expensive to simulate. Salvadori et al. [16] proposed loosely coupled and decoupled approaches to merge the high-fidelity CFD model in a combustor with the RANS model typically used in a turbine.

In the turbine, it is well-known that high turbulence levels and non-uniform temperature profiles can affect vane heat transfer, although many studies intentionally consider uniform inlet velocity at the turbine inlet plane. A series of studies by Ames (Ames [17], Ames et al. [18], Ames et al. [19]) found that the heat transfer at the stagnation and on the pressure side of the vane is heavily augmented by large-scale high-intensity turbulence. Radomsky and Thole [20] simulated combustor-relevant freestream turbulence levels of 20% and concluded that turbulence levels do not decay in the vane passage, but rather remain elevated and continue to augment heat transfer along the entire surface of the vane. More sophisticated combustor-turbine simulators have come online recently (Barringer et al. [21], Povey and Qureshi [22], Basol et al. [23]), underscoring the interest in capturing combustor-turbine interactions at higher fidelity.

This study computationally replicates the non-reacting experimental study of Vakil and Thole [4], which has a simple combustor geometry and well-defined boundary and geometry conditions. For the purpose of validation of the study at hand, the effects of reacting flow are considered to be secondary relative to the significant flow disturbance of the dilution jets. The unique aspect of this work is the consideration of the dilution jet flowfield on the spatially and temporally resolved vane heat transfer, and the effects of dilution hole position.

III. Computational Setup

The combustor simulator of Vakil and Thole [4], modeled in this study, is shown in Figure 1, including the large low speed wind tunnel that the simulator is attached to. The tunnel has temperature conditioning heat exchangers and an electric heater upstream of the combustor simulator to generate temperature variation between core and dilution flow. The linear simulator is periodic in the pitchwise (Y) direction, which enables a single vane to be modeled in this study, conserving computational resources. The combustor simulator has two rows of large dilution holes, with one hole in the first row and two half-holes in the second row (in a periodic mesh straddling the vane), and is designed to simulate a typical aeroengine RQL combustor in both the convergence geometry and the fluid dynamic scaling (momentum flux ratios, dilution mass addition). For this study, no combustor liner effusion holes are modeled; these

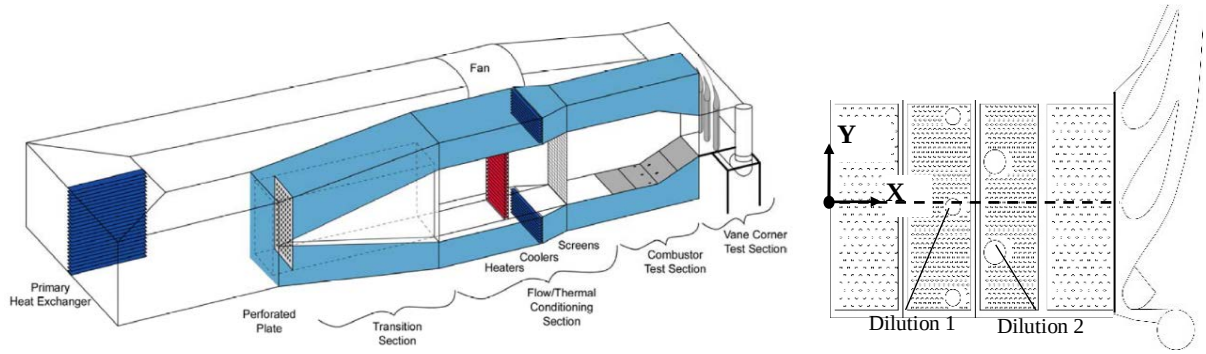

Figure 1. Experimental facility and combustor simulator geometry of Vakil and Thole [4], modeled in this study.

are not expected to have an impact on the dilution jet trajectory or the mixing in the midspan of the tunnel. The vane is based on an aeroengine first vane (Kang et al. [24]), and is located directly downstream of the combustor simulator. Dilution flow conditions for Vakil and Thole [4] are shown in Table 1.

Table 1. Dilution flow conditions of Vakil and Thole [4], used in this study

	% Mass Flow Addition Based on Local Flow Rate	Momentum Flux Ratio Based on Local Mass-Averaged Velocity	Mass Flux Ratio Based on Local Mass-Averaged Velocity	Density Ratio Based on Upstream Flow Conditions	Ratio of Mass-Avg Velocity to Domain Inlet Velocity
Dilution 1	18.5	128	12	1.12	1
Dilution 2	12.5	32	6	1.12	1.6

The computational mesh of the combustor simulator and vane was generated in Pointwise, and was solved in ANSYS Fluent, version 16.1. The computational domain is shown in Figure 2. The periodicity in the experiment was exploited in the domain development. For all simulations in this study, the computational mesh was structured (hexahedral) in the vane boundary layer, with the first gridpoint from the vane surface at a y^+~1 and an expansion ratio of 1.3. Unstructured (tetrahedral) mesh was employed throughout the rest of the domain.

Boundary conditions for the model were set to the same conditions as the experiment, including the inlet velocity to the domain. Dilution plenums were constructed for each hole, to provide independent control over the dilution flowrates. Mass flow inlet boundary conditions were set on each of the dilution plenums, to the same conditions as the Vakil and Thole [4] study (see Table 1). All other surfaces were modeled as no-slip adiabatic walls. The vane surface was modeled as adiabatic. Properties for air were as follows: density was calculated with the incompressible ideal gas law, viscosity with the Sutherland model (function of temperature), specific heat was constant at 1006.43 J/kg*K, thermal conductivity was constant at 0.0242 W/m*K, and molecular weight was 28.933 kg/kmol.

The solution-based grid adaption feature in ANSYS Fluent was used to refine the mesh locally in regions of high gradients, such as the jet shear layers shown in Figure 4a, to improve resolution and study grid convergence. The computational meshes of the original configuration were refined by velocity gradient to increase grid size by 10% of total cell count of the previous mesh. Figure 3 shows area-averaged quantities of nondimensional turbine inlet velocity magnitude and nondimensional vane surface temperature. The difference between the largest mesh sizes (16.2 million and 17.9 million cells) was less than 0.5%. The cause of the anomalous behavior for the 14.8 million cell mesh in Figure 3 is not clear but is under investigation. The grid size used for all RANS cases in this study was 17.9 million cells.

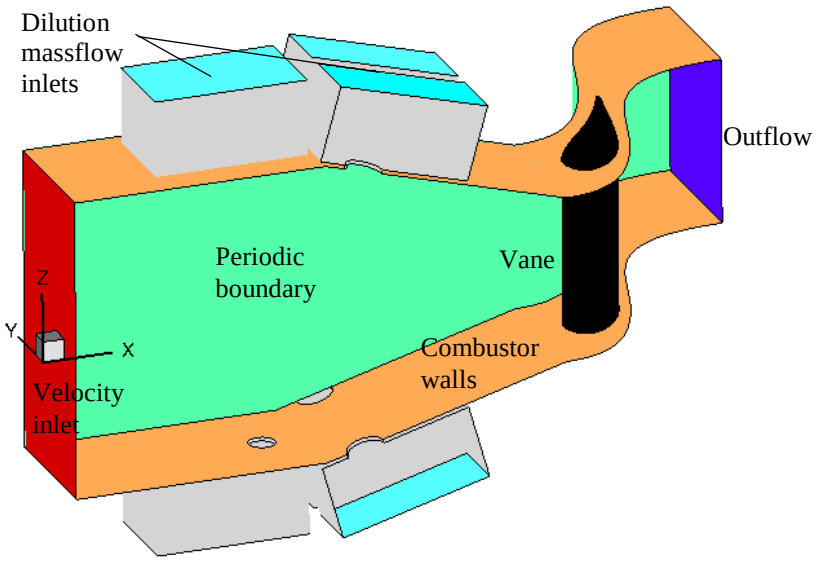

Figure 2. Periodic model of combustor simulator, including supply plenums for dilution flow.

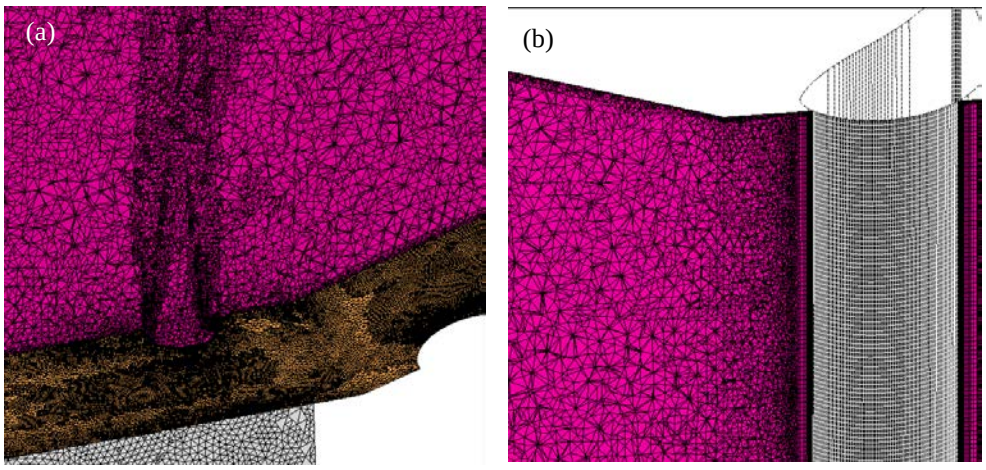

Figure 4. Computational mesh after velocity gradient adaption at (a) dilution centerline and (b) near the vane leading edge.

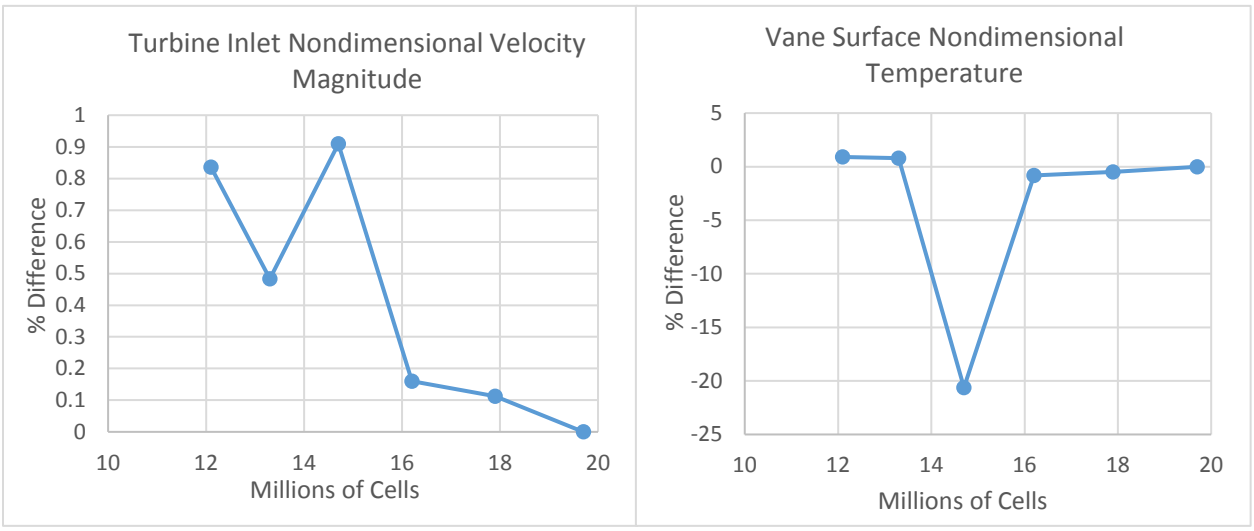

Figure 3. Area averaged quantities of turbine inlet velocity and vane surface temperature for each mesh size in the grid refinement study for the steady RANS models.

A. Steady RANS Simulations

An initial study of the effect of dilution hole position on turbine inlet flow uniformity and vane surface temperature was done using a steady Reynolds-Averaged Navier-Stokes (RANS) approach. The continuity, momentum, and the energy equation were solved with the SST k-omega turbulence model (Menter [25]) available in Fluent. The pressure-based formulation of the equations was employed, with second-order spatial discretization and upwinding for convective terms. The SIMPLE pressure-velocity coupling scheme was used in the solution. Model constants were not varied from the default values in the Fluent solver. The steady simulations were generally run for at least 12,000 iterations or longer, and declared converged when residuals were less than 10^{-4} (energy less than 10^{-6}) and were unchanging for at least two hundred iterations. Several other checks were also performed to determine convergence of the solution, including monitoring the area average pressure and temperature at the turbine inlet plane.

In all, five dilution hole configurations were studied, as shown in Figure 5. The baseline configuration based on Vakil and Thole [4] had dilution jets that were directly in-line with each other on the top and bottom walls of the simulator (referred to as directly opposed). Two other directly opposed cases were analyzed: a shift of the baseline pattern toward the vanes by 50% of the streamwise distance to the vane (referred to as short mixing length), and a

case with a dilution pattern that was shifted both in the streamwise direction (short mixing length) and in the pitchwise direction by 50% of the domain width, simulating clocking of the vane relative to the dilution pattern.

Two other cases were studied where the upper and lower dilution hole patterns were offset from each other by 50% of the domain width, which is more typical of combustor dilution designs. For these offset cases, one was the original configuration offset with a 50% pitchwise shift, and the other was that same pattern shifted streamwise (short mixing length). The combination of cases investigates the effect of directly opposed versus offset dilution hole patterns, as well as the effect of streamwise mixing length, on the uniformity of the flow entering the turbine.

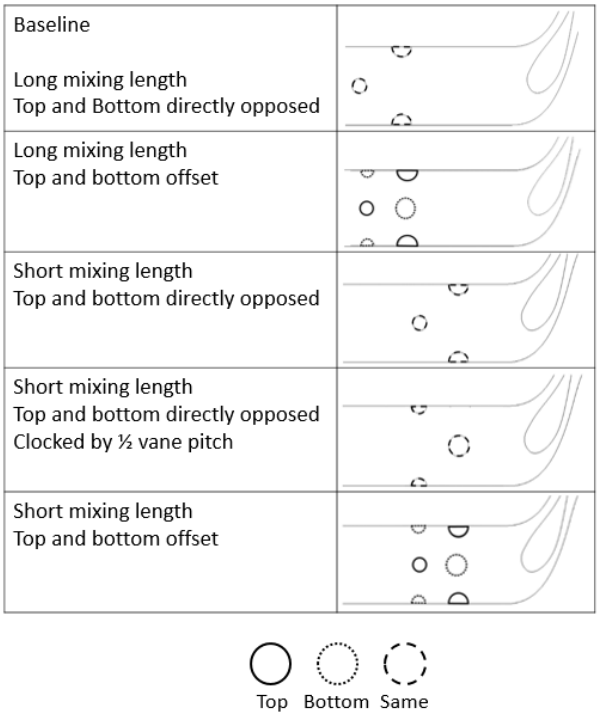

Figure 5. Dilution configurations for steady RANS cases.

B. Time-Resolved Simulations

Time-variant simulations of the baseline model were also examined in this study using the Delayed Detached Eddy Simulation (DDES) model available in Fluent. This method resolves turbulent structures in the main flowfield and models turbulence near the wall using unsteady RANS with an SST k-omega turbulence model. DDES was deemed more practical for this flowfield than a full LES simulation because of the reduced resolution requirements, and because the details of the boundary layer were of less interest than the evolution of the turbulent structures in the main flowfield.

The model for the DDES simulations was identical to that shown in Figure 2, with the same boundary conditions and dilution configuration as the baseline RANS study. Two mesh sizes were examined, with a nominal mesh of 12 million cells based on grid refinements from a RANS study, and a refined mesh with 25 million cells. To obtain the refined DDES mesh, the turbulent dissipation from a baseline RANS model was used to estimate the Kolmogorov length scale per Eq. (1), and the adaption tools in Fluent were used to split cells with a ratio of cell size (determined as cube root of cell volume) to Kolmogorov length scale > 100 (Agarwal et al. [26]).

$$\eta = \left(\frac{\nu^3}{\varepsilon}\right)^{\frac{1}{4}} \qquad \text{Eq. (1)}$$

Figure 6 shows a centerline slice through the combustor, with contours of the ratio of cell size to estimated Kolmogorov scale, for the nominal and refined DDES grids. The refinement was primarily in the dilution zone, and for these time-resolved cases with a more accurate prediction of turbulent dissipation, a cell size/Kolmogorov ratio below 100 is mostly achieved for the refined DDES, with some regions near the dilution jets that could still be refined.

The DDES simulations used a production limiter option available in Fluent, and default model constants. For the nominal mesh size of 12 million cells, a timestep of $2\text{x}10^{-4}$ seconds was employed, so that the maximum convective Courant number is approximately one. Unsteady simulations were run for five flow-through times in the domain (approximately 0.6 seconds for a single flow-through time) before sampling, to ensure a statistically stationary flow. Monitors of velocity and temperature were employed throughout the flowfield to check statistical stationarity. After the simulation was determined to be statistically stationary, flow samples were collected for nine flow-through times. Figure 7 shows a comparison of the mean and RMS of streamwise velocity at the turbine inlet plane, at the end of the eighth flow-through time versus the end of the ninth flow-through time. Only minor differences are noted between the results, suggesting temporally converged statistics.

The refined DDES simulation required a time step of $1.2\text{x}10^{-4}$ seconds to achieve a maximum convective Courant number of 1. Due to computing resource limitations, only two flow-through times were computed before beginning statistical sampling, and the total sample time was only 2.5 flow-through times. All other model constants and boundary conditions were identical to the nominal DDES case.

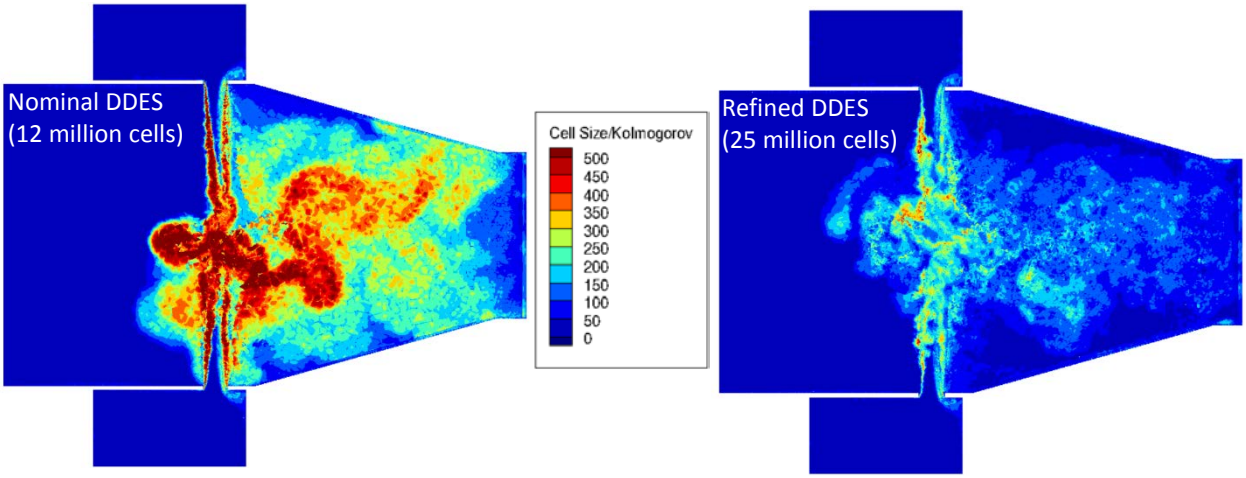

Figure 6. Ratio of cell size to Kolmogorov length scale for nominal DDES (left) and refined DDES (right) at the centerline.

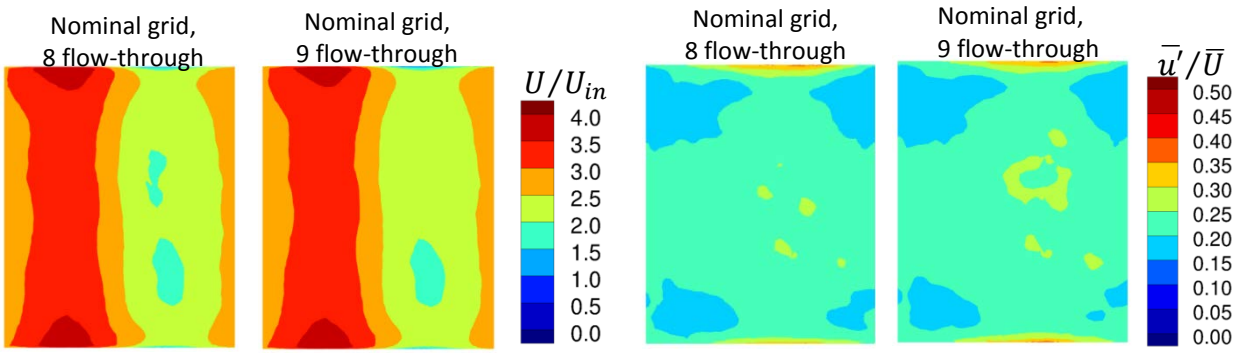

Figure 7. Mean and RMS of streamwise velocity at the turbine inlet plane for flow sampling over 8 versus 9 flow through times, for the nominal grid DDES case.

IV. Comparison to Other Results

The study by Vakil and Thole [4] modeled both dilution and combustor liner film cooling effects. The effects of film cooling are disregarded in this study as dilution flow dominates the flowfield and the majority of the coolant mass flow is supplied to the dilution holes. Figure 9 compares the trajectory of the first row dilution jet (on a plane passing through the center of the jet) for the steady RANS, the time-average of the nominal DDES, and the experimental results of Vakil and Thole [4]. The prediction of the jet trajectory using a correlation by Lefebvre and Ballal [27] is overlaid on each case. The DDES case follows the theoretical trajectory almost exactly, with the steady RANS jet also well-approximated by the correlation. These stand in sharp contrast to the experimental measurements, which show the jet being bent significantly by the main flowfield and penetrating to a lower span height. The reason for the discrepancy is not clear; several checks were performed to compare the total mass addition as well as the local momentum flux of the dilution jets to the values reported in Vakil and Thole [4], which all agreed.

Interestingly, a prior computational study by Stitzel and Thole [28] of the same combustor simulator used by Vakil and Thole [4] produced results with similar trends to the current study. As seen in Figure 8, the computation by Stitzel and Thole [28], which used steady RANS with an RNG k-ε turbulence model and symmetry planes at the combustor midspan, also shows strong jet overpenetration and a large recirculation region upstream of the first row of dilution holes. Note that the streamlines for the cases from our study are not enforced to be symmetric; because of this, the steady RANS computations exhibited sensitivity to small mispredictions of the dilution jet trajectories.

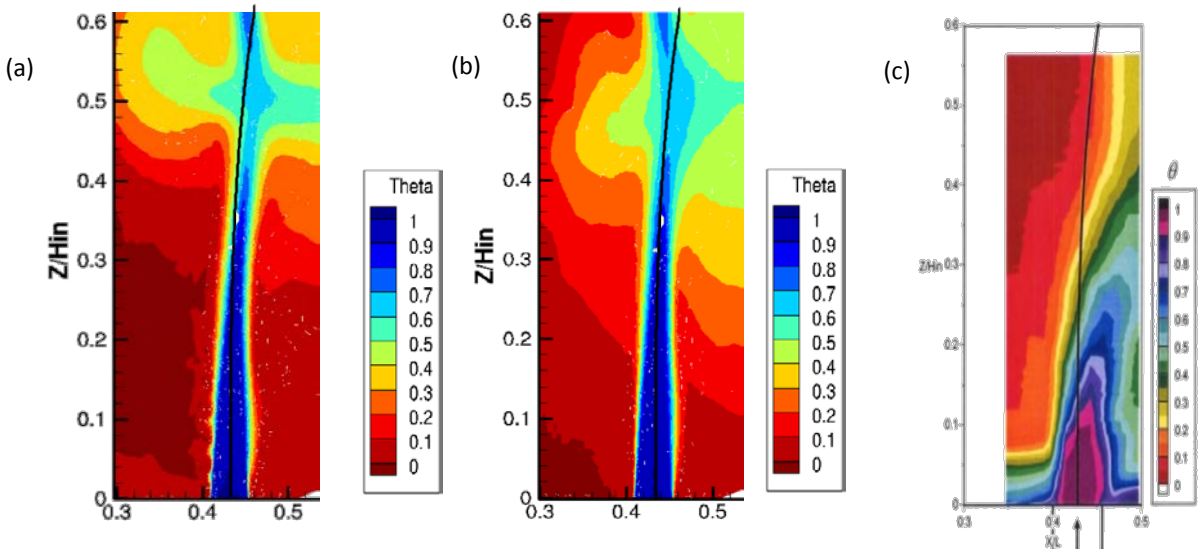

Figure 9. Midpitch plane for the first row dilution hole, with a jet penetration correlation by Lefebvre and Ballal [27] for (a) steady RANS, (b) time-average of nominal DDES, (c) experimental result of Vakil and Thole [4].

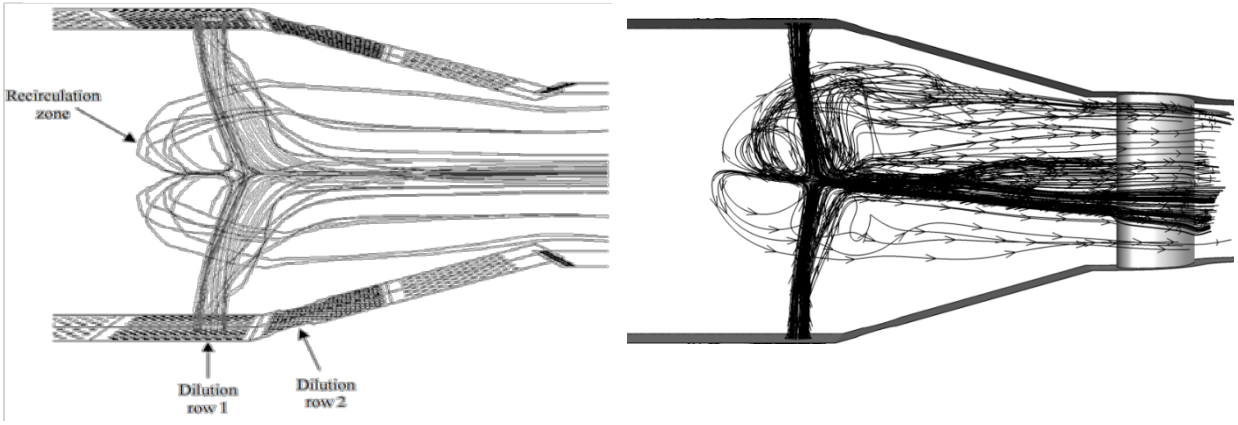

Figure 8. Comparison of first row dilution hole streamlines for Stitzel and Thole [28] (left) and this study (right).

V. Results

This section first describes the impact of dilution hole location on the turbine inlet flow uniformity using steady RANS simulations. Then, the RANS solution for the baseline configuration is compared to a DDES calculation on the nominal grid size. Finally, the effect of grid refinement on the DDES solution result is investigated.

A. Effect of Dilution Hole Location

Figure 10 shows the steady RANS predictions of the effect of dilution hole location on the nondimensional surface temperature of the combustor walls and the turbine vane. Isosurfaces of nondimensional temperature at θ=0.55 are also shown, to indicate the trajectory of the dilution jets. For the baseline case with directly opposed jets, the RANS model predicts very strong jet penetration (I=128 for the first row), with jets that impact each other in the midspan of the combustor. Since most of the cooling flow interacts at the midspan, there is little to no coolant on the combustor wall or the turbine endwall surfaces (recall liner effusion cooling is not modeled in this study). However, the RANS

model predicts a distinct band of cooler fluid on the vane at its centerline. This coolant distribution is not ideal for turbine durability due to both the hot zones near the endwalls, as well as temperature gradients between the endwall and center that would cause differential thermal expansion and cracking issues.

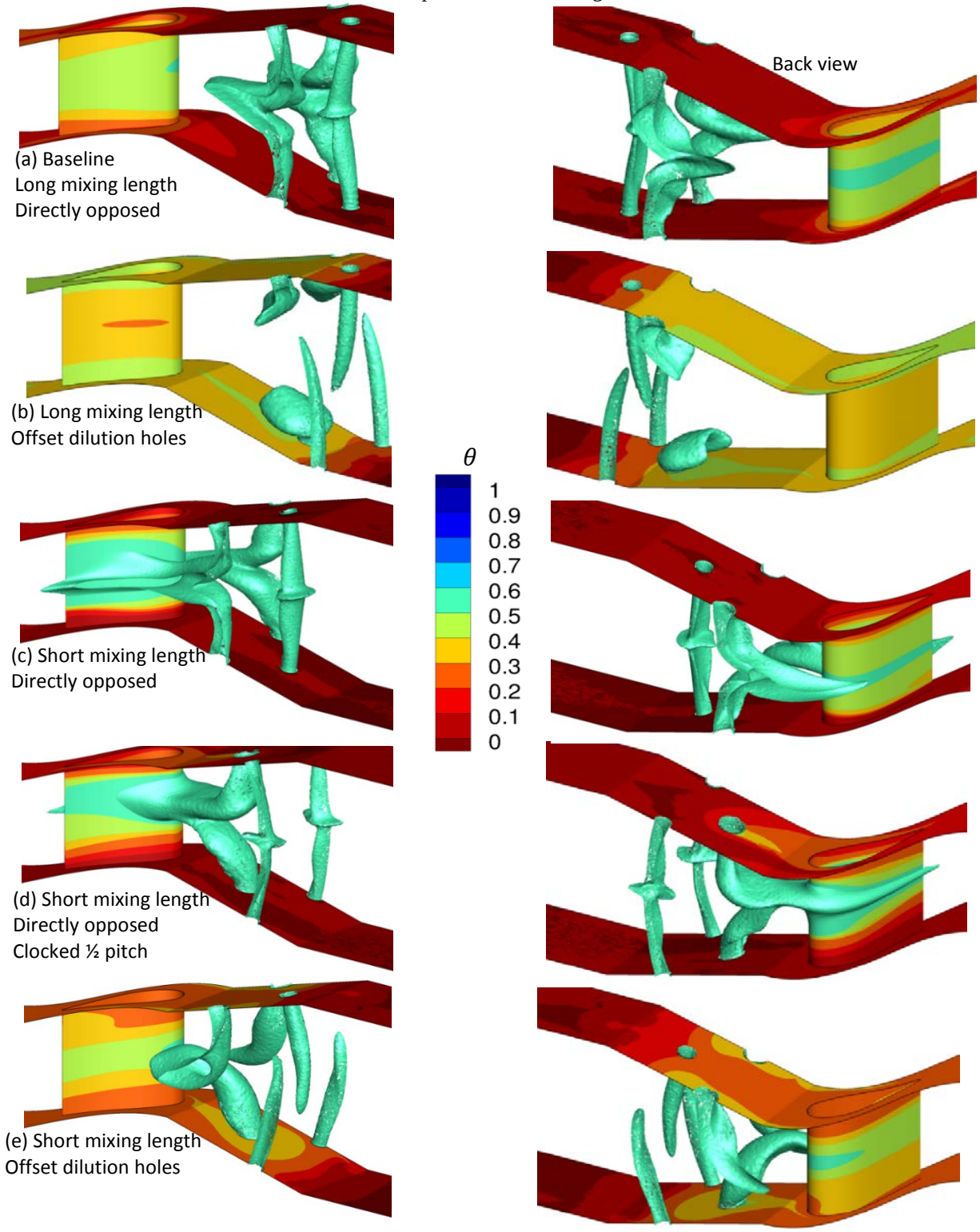

Figure 10. Nondimensional surface temperature, and isosurface of temperature at θ=0.55, for the dilution hole positions.

The opposed jet configuration with the long mixing length in Figure 10b shows very little interaction between jets in a given row, but there appears to be a significant interaction between the first row jet and a second row jet, whereby the second row jet at a lower effective momentum flux (I=32) is pressed down toward the wall. Because of this, the combustor wall and turbine endwall temperatures are cooler than in the baseline case, but the vane airfoil temperature is warmer.

The remainder of the cases in Figure 10 are for the short mixing length, where the dilution pattern is shifted toward the turbine vane by 50% of the distance to the vane. In the directly opposed case with the short mixing length, the second row dilution jets are predicted to impact directly on the vane pressure side and provide a significant amount of cooling. This may be a possible advantage in a short combustor design, whereby airfoil cooling could be reduced because of the dilution cooling. When the dilution pattern is clocked by ½ of a vane pitch, the large second-row dilution hole directly impacts the vane leading edge, causing even more cooling on the airfoil surface. However, all of the directly opposed cases for this short mixing length result in little to no cooling on the combustor walls or turbine endwalls, which creates severe temperature gradients in the vane. It is likely there would need to be some significant cooling present for those surfaces (as is typical in current aeroengines, although not modeled here).

Finally, the effect of a short mixing length with an offset dilution hole pattern is seen in Figure 10e. As for the long mixing length, an offset dilution hole pattern results in strong jet penetration for the first row. Unlike for the long mixing length, the second row dilution jets in the short mixing length pattern are not suppressed by upstream jets, and also penetrate into the mainstream. This results in better mixing and more uniform distribution of wall temperatures on the airfoil and endwall surfaces, relative to the directly opposed configurations for the short mixing length.

Often in turbine design, spatially- or circumferentially-averaged quantities (velocity, turbulence, temperature) are provided from higher-fidelity unsteady simulations. However, this can mask the complexity of the incoming flow and lead to mispredictions of vane temperature if non-uniformity is not properly understood. Figure 11 shows the mean streamwise velocity (axial direction) through the turbine inlet plane for the various dilution patterns examined. Note that the normalization parameter in Figure 11 is the mass-average streamwise (x-direction) velocity over the entire plane at this location. The plane is located about 18% of the vane chord upstream of the vane leading edge, and the view in the figures is looking upstream toward the dilution jets. Because of dilution flow mass addition and flow acceleration, the mass-average streamwise velocity at this location is approximately 2.7 times the domain inlet velocity. Note that the turbine inlet plane contours are not perfectly symmetric around the midspan, which would

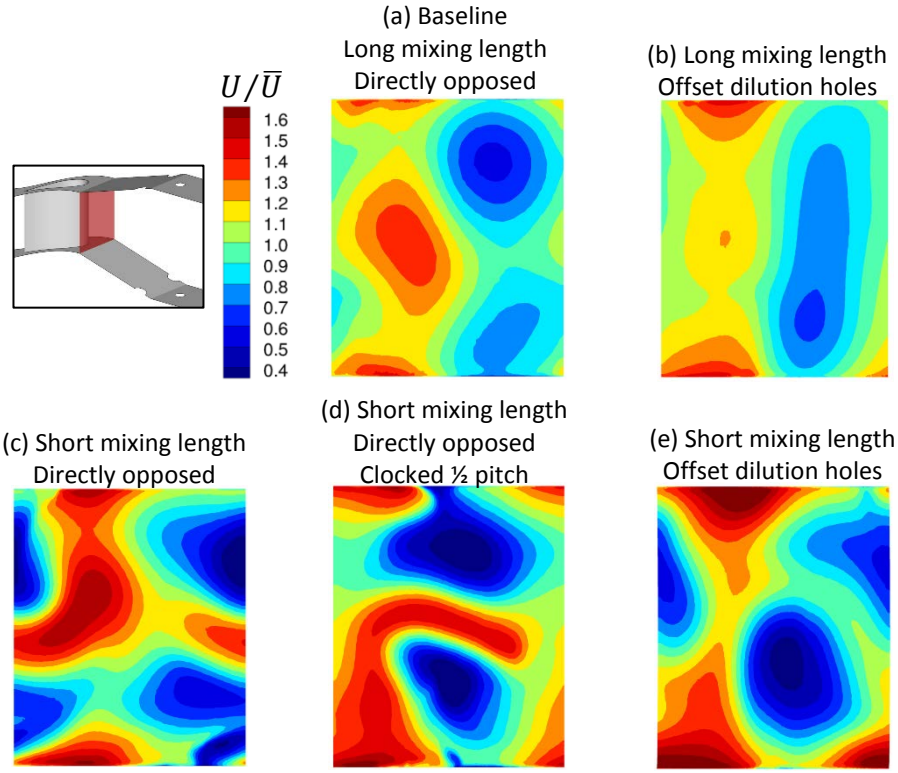

Figure 11. Mean velocity at the turbine inlet plane (see inset, views are looking upstream) for the dilution configurations.

normally be expected. Although the RANS cases had low residuals and were considered converged by the metrics described earlier, the solutions were prone to instability due to the difficulty of the RANS model in capturing the time-average behavior of a highly unsteady phenomenon.

For the baseline case in Figure 11a, the turbine inlet velocity shows some non-uniformity associated with the dilution jet trajectories, with two low-velocity regions near the endwall and a high-velocity region near the center. The variation in streamwise velocity can be up to ±40% relative to the mass-average velocity. In comparison, the offset case with the long mixing length (Figure 11b) shows a minor improvement in velocity uniformity across the turbine inlet plane.

For the short mixing length cases in Figure 11, there are much stronger non-uniformities in the turbine inlet velocity, as might be expected because of the shorter distance between the jets and the turbine inlet. For the directly opposed case that was clocked ½ vane pitch, the inlet velocity can vary more than ±60% relative to the average. The effect of clocking the dilution pattern, specifically the low-velocity wake of the large second-row jet, is visible when comparing Figure 11c versus Figure 11d. For the offset case with the short mixing length (Figure 11e), there are regions of very high streamwise velocity near the top and bottom walls, which are the remnants of a dilution jet from one wall impacting the opposite wall. This may not be advantageous for effusion cooling schemes on the combustor walls, since the jet flow could strip off or disturb the effusion.

Figure 12 shows the local turbulence intensity predicted by the RANS model at the turbine inlet plane for the various dilution configurations. Local turbulence intensity is calculated by taking the square root of the local turbulent kinetic energy, and normalizing by the same mass-average turbine inlet plane velocity. The baseline case with the directly opposed jets (Figure 12a) shows turbulence levels of up to 35% at the midspan of the turbine inlet, with low levels of turbulence near the endwall. In contrast, the offset case for the long mixing length (Figure 12b) has more uniform turbulence distribution, with levels nominally below 30% at midspan but higher turbulence closer to the top and bottom walls. Increased turbulence near the walls could increase heat transfer coefficients on those surfaces, or disperse endwall coolant.

The short mixing length cases in Figure 12 have more non-uniform distributions of turbulence intensity, relative to the long mixing length cases. For the directly opposed short mixing length cases, turbulence levels are highest in the center of the turbine inlet plane, with levels up to 45%. This is much higher than the more commonly assumed level of approximately 20% from prior studies (Barringer et al. [2], Ames et al. [29], Van Fossen and Bunker [30],

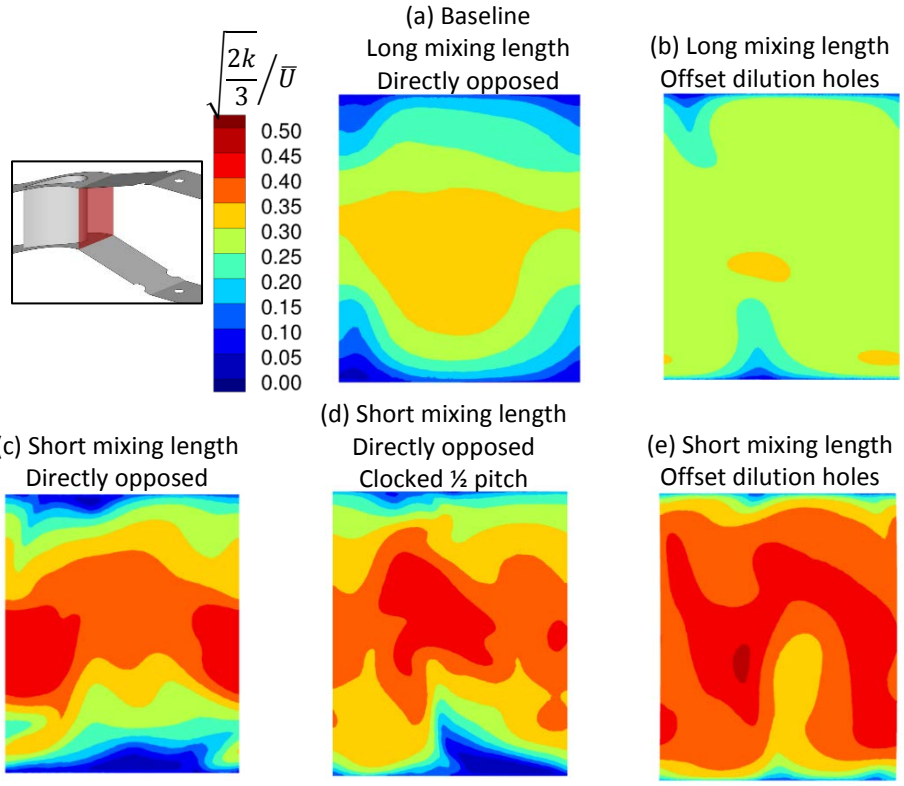

Figure 12. Local turbulence intensity at the turbine inlet plane (see inset) for the dilution configurations.

Goebel et al. [31]), although more recent experimental studies for both RQL-style (Leonetti et al. [32]) and swirl-stabilized combustors (Cha et al. [15]) indicate that turbulence levels may actually exceed 35%. The offset case for the short mixing length (Figure 12e) has the highest overall turbulence intensity, with levels of 30% even close to the upper and lower turbine endwalls. While these high levels of turbulence are beneficial for mixing of combustion products, they can increase convective heat transfer on the airfoil and endwall surfaces and may need to be accounted for in a durability design.

B. Comparison of steady RANS versus DDES

The time-average result (total of nine flow-through time samples, or 5.4 seconds) from the nominal-grid DDES solution of the baseline case is shown in Figure 13. It is immediately apparent by comparing the isosurfaces of nondimensional temperature between the baseline in Figure 10a and Figure 13a that the dilution jets do not retain coherency as far downstream in the DDES time-average result. This is due to the more accurate prediction of mixing in the time-resolved DDES case. Another important difference is the endwall temperature in the vane passage, which is lower for the DDES versus the RANS case due to increased mixing of the dilution flow.

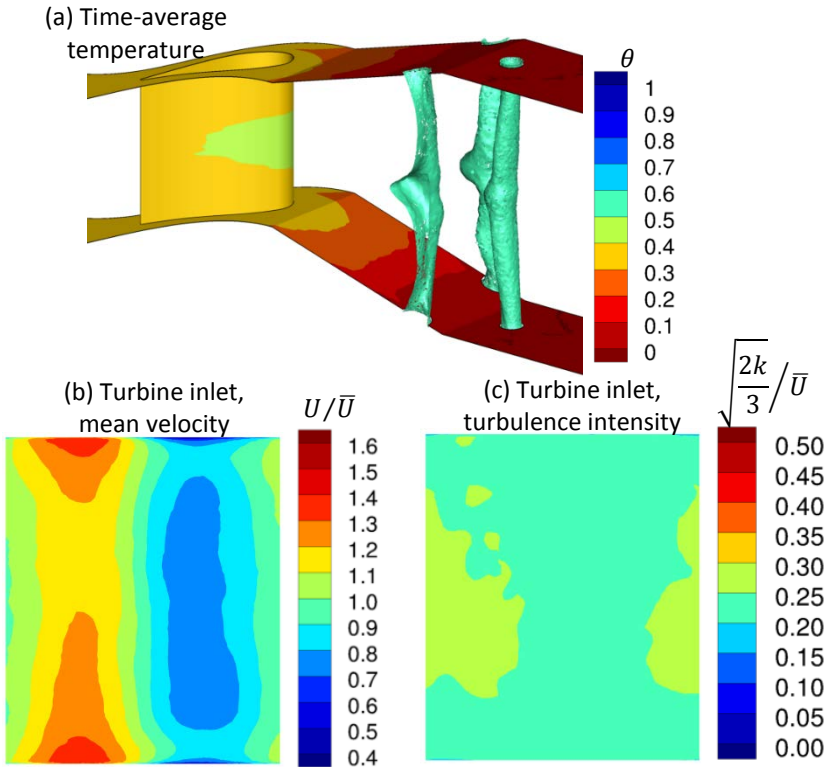

Figure 13. Time-average results for the DDES solution of the baseline geometry on the nominal grid of 12 million cells.

At the turbine inlet plane, the mean streamwise velocity is more uniform in the spanwise (vertical) direction for the DDES (Figure 13b) versus RANS (Figure 11a), again due to the better mixing, but there is still a distinct difference in velocity between the right and left sides of the plane. This is due to the pressure field of the vane at this location, which slows down the approaching fluid on the right (pressure side of the vane) and increases it on the left (accelerating around the suction side of the vane). The turbulence intensity is also more uniform, and lower in magnitude near the midspan (~25%), for the DDES simulation (Figure 13c) relative to the RANS case (Figure 12a). Interestingly, the turbulence intensity is predicted to be higher near the upper and lower endwalls, in the DDES case. Thus, a RANS simulation of this dilution configuration would perhaps underpredict the level of heat transfer enhancement on the turbine endwalls.

The instantaneous behavior of the flow from the DDES case is shown in Figure 14, for the surface temperature and the turbine inlet plane. The rollup of the first-row dilution jet shear layer is apparent in the isosurfaces in Figure 14a. Also, a fairly significant hotspot is shown on the vane pressure side surface near the trailing edge. However, due

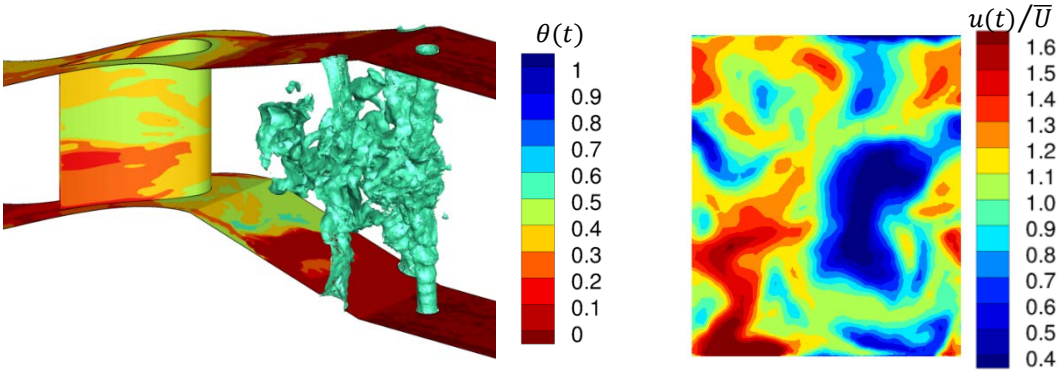

Figure 14. (a) Instantaneous temperature (isosurfaces at θ=0.55) and (b) instantaneous streamwise velocity at the turbine inlet plane.

to the thermal capacitance of the metal in a turbine vane in the engine, this instantaneous increase in adiabatic wall temperature would not likely have an impact on the operational metal temperature; Figure 13a indicates only a modest difference in time-average temperature over the vane surface. At the turbine inlet plane, Figure 14b indicates a wide range of turbulent structures entering the turbine, with instantaneous velocities that are up to ±60% of the time- and space-average value of $\overline{U} = 4.41$ m/s.

Since the temperature fluctuations are also temporally resolved in the DDES simulation, it is interesting to understand where the fluctuations are the largest on the surfaces of interest (combustor walls, turbine airfoil). Figure 15 shows a semi-transparent isosurface of instantaneous θ at a level of 0.4, as well as contours of the RMS of fluctuations in surface temperature. Here, it is apparent that the region that would be most highly distressed by fluctuating temperatures is the combustor convergence immediately downstream of the dilution jets. The vane centerline shows the lowest fluctuations in surface temperature, although the upper and lower vane passage endwalls are slightly higher. These are regions of higher uncertainty in local adiabatic wall temperature, and could be accounted for in a statistically-based durability design.

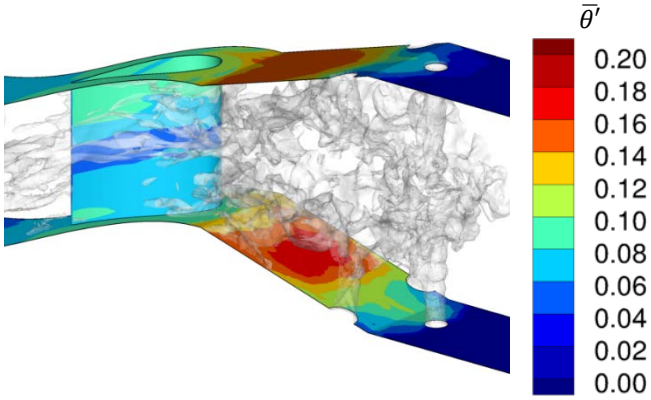

Figure 15. Isosurfaces (semi-transparent) of instantaneous θ=0.4, with surface contours of RMS of θ.

Also of interest to turbine design is the correctness of representing the inlet turbulence condition via a single quantity, namely the turbulent kinetic energy, *k*. Figure 16 shows the RMS of the streamwise, pitchwise, and spanwise velocity components from the DDES model at the turbine inlet plane. If the components are all equivalent, the turbulence field would be isotropic and could be represented by a single quantity. However, this does not appear to be

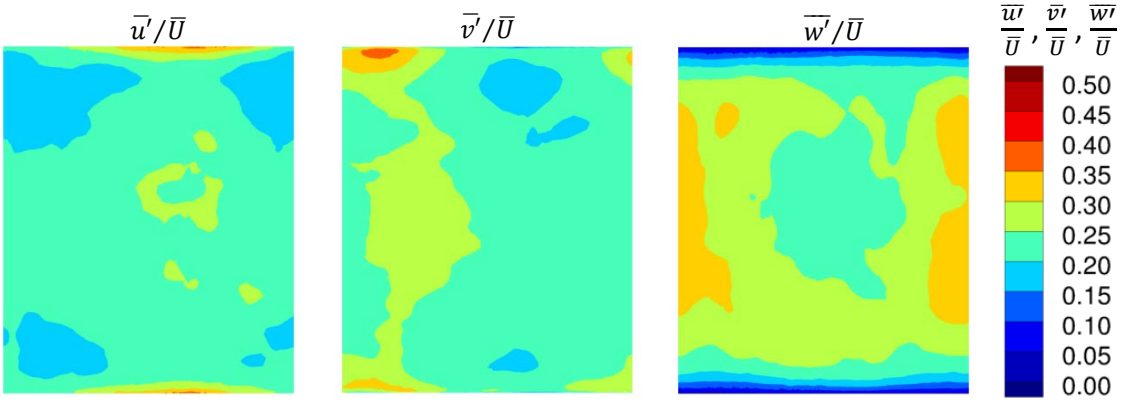

Figure 16. Streamwise (u), pitchwise (v), and spanwise (w) velocity fluctuations at the turbine inlet plane.

the case for this baseline configuration. In particular, the spanwise velocity fluctuations are about 30% larger than the streamwise fluctuations at the sides of the turbine inlet plane. Possibly this is due to the pressure field of the vane causing vortex stretching around the vane leading edge, or due to lack of sufficient distance for the wake breakdown of the second row of dilution holes. At the least, the turbulence is certainly not isotropic near the upper and lower endwalls, which would impact the ability of a RANS model to properly predict that effect on surface temperature.

C. Effect of DDES grid refinement

As described earlier, the DDES grid was refined using local adaption based on the ratio of the cube root of cell volume to the local Kolmogorov length scale. The impact of this refinement was primarily in the initial dilution zone, but it was not clear how this might impact the convection and dissipation of turbulent scales entering the turbine. Figure 17 shows the time-average results for the refined DDES case, plotted in the same way as Figure 13. Note that due to computational resource restrictions, the refined DDES has not yet been sampled for an equivalent amount of time and there is more uncertainty in the average and RMS quantities.

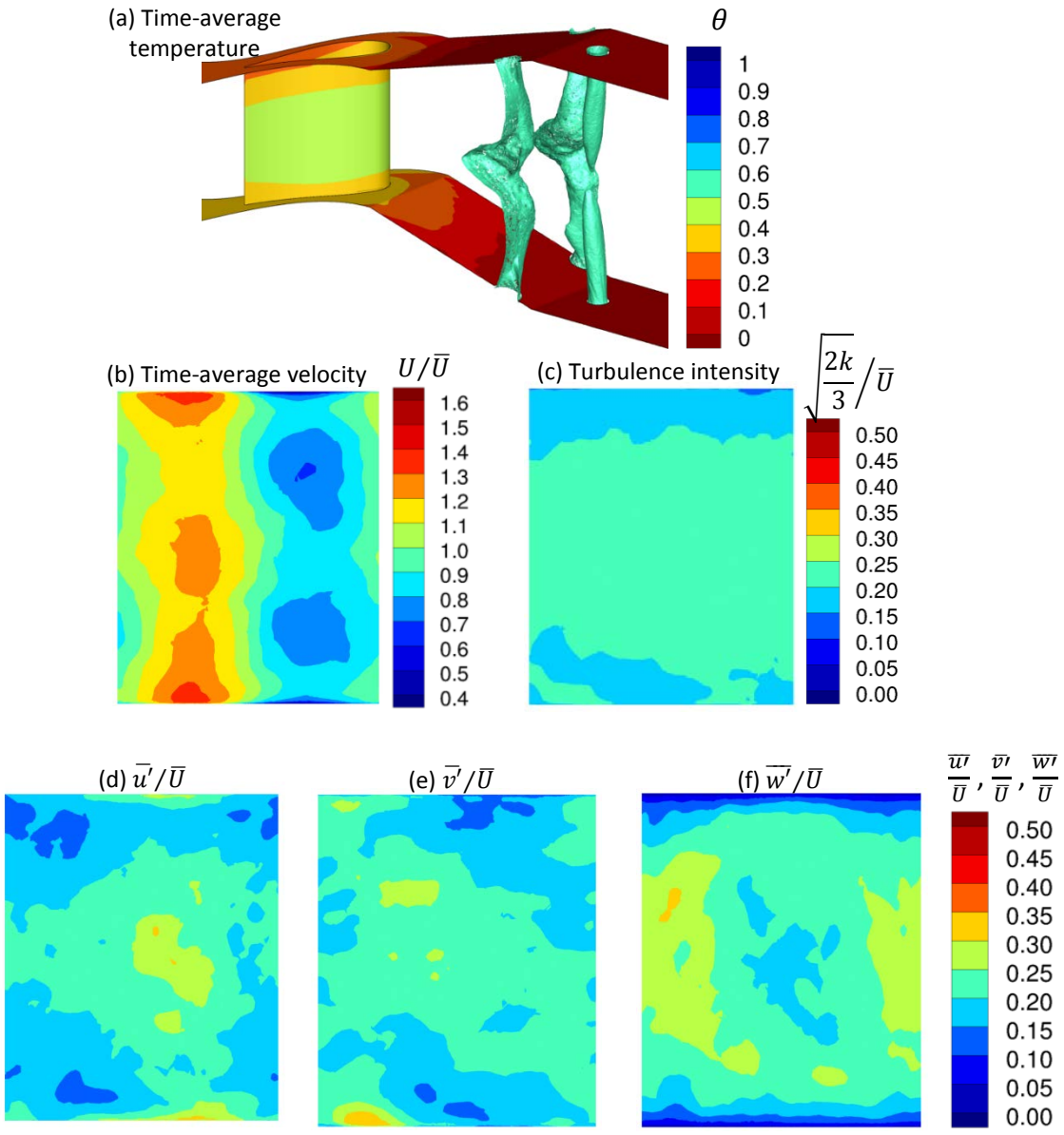

Figure 17. Time-average results for the refined DDES grid (25 million cells).

The isosurfaces of θ are similar in terms of jet trajectory between Figure 13a and Figure 17a, although the refined DDES predicts that the time-average jet profile from the second row of dilution will persist further downstream. This is likely because the refined model is better capturing the range of scales of the turbulent dissipation of the jets, whereas the coarseness of the nominal DDES grid results in additional numerical dissipation. The effect on the vane surface temperature is minor, with slightly lower temperature predicted by the refined DDES case.

The time-average turbine inlet plane quantities in Figure 17b-f compare fairly well to the nominal DDES results in Figure 13b-c and Figure 16, although the refined DDES predicts slightly lower turbulence levels near the upper and lower endwalls. The reason for this is not yet clear, but could be partially due to inadequate sampling time for this larger case. In general, the effect of the grid refinement performed here does not appear to have a significant impact on the prediction of turbine inlet quantities.

VI. Conclusions

A computational study of an RQL-style combustor-turbine configuration was performed using steady RANS and time-dependent DDES calculations. The effect of dilution hole position on the downstream turbine vane was investigated using steady RANS. The baseline configuration was also investigated using DDES, to resolve turbulent scales of the large dilution jets, and compared to the RANS baseline. Finally, a refined DDES model was run to determine if turbine inlet quantities were impacted by increased resolution in the dilution jet region.

The steady RANS models indicated better uniformity but higher overall turbulence levels for dilution jet configurations where the upper and lower jets were offset, relative to jets with centerlines directly opposed to each other. Shifting the dilution jets 50% closer to the vane resulted in increased inlet flow non-uniformity and very high turbulence levels, as well as creating more significant temperature gradients on the vane and endwall surfaces downstream of the jets. It appears that dilution jets located close to the vane might be useful for vane cooling, but more work should be done to understand surface convective heat transfer coefficients, which would likely increase.

As expected, the DDES simulation predicted more mixing of the dilution jet than the steady RANS result, so that the turbine vane and endwall surface temperatures were more uniform. Turbine inlet velocity and turbulence level was also more uniform, although turbulence levels were still high (~25%). Evaluation of the individual fluctuating velocity components indicates that the incoming turbulence is anisotropic, particularly closer to the vane endwall surfaces, which cannot be captured by a RANS approach. The effect of the turbulence anisotropy and its propagation through the turbine should be investigated in more detail. Refinement of the DDES grid around the initial injection of the dilution jets appeared to have a minor impact on the predicted turbine inlet quantities.

This study indicates the importance of properly resolving turbulent structures and their propagation to accurately simulate conditions for the first vane. Future work should investigate the predicted turbulent length scales, and how to utilize non-uniform inlet conditions in a RANS approach to improve accuracy of turbine vane temperature predictions.

VII. References

[1] Fric, T. F., and Roshko, A. "Vortical Structure in the Wake of a Transverse Jet," *Journal of Fluid Mechanics,* Vol. 279, 1994, pp. 1-47. doi: 10.1017/S0022112094003800

[2] Barringer, M. D., Richard, O. T., Walter, J. P., Stitzel, S. M., and Thole, K. A. "Flow Field Simulations of a Gas Turbine Combustor," *Journal of Turbomachinery,* Vol. 124, No. 3, 2002, pp. 508-516. doi: 10.1115/1.1475742

[3] Epstein, A. H. "Aeropropulsion for Commercial Aviation in the Twenty-First Century and Research Directions Needed," *AIAA Journal,* Vol. 52, No. 5, 2014, pp. 901-911. doi: 10.2514/1.J052713

[4] Vakil, S. S., and Thole, K. A. "Flow and Thermal Field Measurements in a Combustor Simulator Relevant to a Gas Turbine Aeroengine," *Journal of Engineering for Gas Turbines and Power,* Vol. 127, No. 2, 2005, pp. 257-267. doi: 10.1115/1.1806455

[5] Holdeman, J. D., and Walker, R. "Mixing of a Row of Jets with a Confined Crossflow," *AIAA Journal,* Vol. 15, No. 2, 1977, pp. 243-249.

[6] Holdeman, J. D., Srinivasant, R., and Berenfeld, A. "Experiments in Dilution Jet Mixing," *AIAA Journal,* Vol. 22, No. 10, 1984, pp. 1436-1443. doi: 10.2514/3.48582

[7] Stevens, S. J., and Carrotte, J. F. "Experimental Studies of Combustor Dilution Zone Aerodynamics. I - Mean Flowfields," *Journal of Propulsion and Power,* Vol. 6, No. 3, 1990, pp. 297-304. doi: 10.2514/3.25434

[8] Stevens, S. J., and Carrotte, J. F. "Experimental Studies of Combustor Dilution Zone Aerodynamics. II - Jet Development," *Journal of Propulsion and Power,* Vol. 6, No. 4, 1990, pp. 504-511. doi: 10.2514/3.25463

[9] Dai, W., Zhang, Y., Lin, Y., Yang, Q., and Zhang, C. "Influence of the Arrangement of Dilution Holes for Dilution Mixing in a Three-Injector Reverse Flow Combustor," *ASME Turbo Expo 2014: Turbine Technical Conference and Exposition,* 2014.

[10] Cha, C. M., Hong, S., Ireland, P. T., Denman, P., and Savarianandam, V. "Experimental and Numerical Investigation of Combustor-Turbine Interaction Using an Isothermal, Nonreacting Tracer," *Journal of Engineering for Gas Turbines and Power,* Vol. 134, No. 8, 2012, pp. 081501-081501. doi: 10.1115/1.4005815

[11] Di mare, F., Jones, W. P., and Menzies, K. R. "Large Eddy Simulation of a Model Gas Turbine Combustor," *Combustion and Flame*, Vol. 137, No. 3, 2004, pp. 278-294. doi: http://dx.doi.org/10.1016/j.combustflame.2004.01.008
[12] Moin, P., and Apte, S. V. "Large-Eddy Simulation of Realistic Gas Turbine Combustors," *AIAA Journal*, Vol. 44, No. 4, 2006, pp. 698-708. doi: 10.2514/1.14606
[13] Patil, S., and Tafti, D. "Large-Eddy Simulation of Flow and Convective Heat Transfer in a Gas Turbine Can Combustor with Synthetic Inlet Turbulence," *Journal of Engineering for Gas Turbines and Power*, Vol. 134, No. 7, 2012, pp. 071503-071503. doi: 10.1115/1.4006081
[14] Boudier, G., Gicquel, L. Y. M., Poinsot, T., Bissières, D., and Bérat, C. "Comparison of LES, RANS and Experiments in an Aeronautical Gas Turbine Combustion Chamber," *Proceedings of the Combustion Institute*, Vol. 31, No. 2, 2007, pp. 3075-3082. doi: http://dx.doi.org/10.1016/j.proci.2006.07.067
[15] Cha, C. M., Ireland, P. T., Denman, P. A., and Savarianandam, V. "Turbulence Levels Are High at the Combustor-Turbine Interface," *ASME Turbo Expo 2012: Turbine Technical Conference and Exposition*, 2012, Paper GT2012-69130. doi: 10.1115/GT2012-69130
[16] Salvadori, S., Riccio, G., Insinna, M., and Martelli, F. "Analysis of Combustor/Vane Interaction with Decoupled and Loosely Coupled Approaches," *ASME Turbo Expo 2012: Turbine Technical Conference and Exposition*, 2012, Paper GT2012-69038. doi: 10.1115/GT2012-69038
[17] Ames, F. E. "The Influence of Large-Scale High-Intensity Turbulence on Vane Heat Transfer," *Journal of Turbomachinery*, Vol. 119, No. 1, 1997, pp. 23-30. doi: 10.1115/1.2841007
[18] Ames, F. E., Argenziano, M., and Wang, C. "Measurement and Prediction of Heat Transfer Distributions on an Aft-Loaded Vane Subjected to the Influence of Catalytic and Dry Low NOx Combustor Turbulence," *Journal of Turbomachinery*, Vol. 126, No. 1, 2004, pp. 139-149. doi: 10.1115/1.1645867
[19] Ames, F. E., Wang, C., and Barbot, P. A. "Measurement and Prediction of the Influence of Catalytic and Dry Low NOx Combustor Turbulence on Vane Surface Heat Transfer," *Journal of Turbomachinery*, Vol. 125, No. 2, 2003, pp. 221-231. doi: 10.1115/1.1559898
[20] Radomsky, R. W., and Thole, K. A. "Flowfield Measurements for a Highly Turbulent Flow in a Stator Vane Passage," *Journal of Turbomachinery*, Vol. 122, No. 2, 2000, pp. 255-262.
[21] Barringer, M. D., Polanka, M. D., and Thole, K. A. "Effects of Combustor Exit Profiles on Vane Aerodynamic Loading and Heat Transfer in a High Pressure Turbine," *Journal of Turbomachinery*, Vol. 131, No. 2, 2009, pp. 021008-021008. doi: 10.1115/1.2950051
[22] Povey, T., and Qureshi, I. "Developments in Hot-Streak Simulators for Turbine Testing," *Journal of Turbomachinery*, Vol. 131, No. 3, 2009, pp. 031009-031009. doi: 10.1115/1.2987240
[23] Basol, A. M., Kalfas, A. I., Abhari, R. S., and Kai, R. "Integrated Combustor Turbine Design for Improved Aerothermal Performance: Effect of Dilution Air Control," *Journal of Engineering for Gas Turbines and Power*, Vol. 134, No. 9, 2012, pp. 091501-091501. doi: 10.1115/1.4006671
[24] Kang, M. B., Kohli, A., and Thole, K. A. "Heat Transfer and Flowfield Measurements in the Leading Edge Region of a Stator Vane Endwall," *Journal of Turbomachinery*, Vol. 121, No. 3, 1999, pp. 558-568.
[25] Menter, F. R. "Two-Equation Eddy-Viscosity Turbulence Models for Engineering Applications," *AIAA Journal*, Vol. 32, No. 8, 1994, pp. 1598-1605. doi: 10.2514/3.12149
[26] Agarwal, K. K., Konakalla, S. R., and Selvan, S. "On Meshing Guidelines for Large Eddy Simulations of Gas Turbine Combustors," *ASME Turbo Expo 2014: Turbine Technical Conference and Exposition*, 2014.
[27] Lefebvre, A. H., and Ballal, D. R. *Gas Turbine Combustion*: CRC Press, 2010.
[28] Stitzel, S., and Thole, K. A. "Flow Field Computations of Combustor-Turbine Interactions Relevant to a Gas Turbine Engine," *Journal of Turbomachinery*, Vol. 126, No. 1, 2004, pp. 122-129. doi: 10.1115/1.1625691
[29] Ames, F. E., Barbot, P. A., and Wang, C. "Effects of Aeroderivative Combustor Turbulence on Endwall Heat Transfer Distributions Acquired in a Linear Vane Cascade," *Journal of Turbomachinery*, Vol. 125, No. 2, 2003, pp. 210-220.
[30] Van Fossen, G. J., and Bunker, R. S. "Augmentation of Stagnation Region Heat Transfer Due to Turbulence from a DLN Can Combustor," *Journal of Turbomachinery*, Vol. 123, No. 1, 2001, pp. 140-146.
[31] Goebel, S., Abuaf, N., Lovett, J., and Lee, C.-P. "Measurements of Combustor Velocity and Turbulence Profiles," *ASME 1993 International Gas Turbine and Aeroengine Congress and Exposition*, 1993.
[32] Leonetti, M., Lynch, S. P., O'Connor, J., and Bradshaw, S. D. "Combustor Dilution Hole Placement and Its Effect on the Turbine Inlet Flowfield," *AIAA Journal of Propulsion and Power*, (in press), 2016.